



HAL
open science

Wavelet encoding of BRDFs for real-time rendering

Luc Claustres, Loic Barthe, Mathias Paulin

► **To cite this version:**

Luc Claustres, Loic Barthe, Mathias Paulin. Wavelet encoding of BRDFs for real-time rendering. Graphics Interface, May 2007, Montréal, Canada. pp.169-176, 10.1145/1268517.1268546 . hal-01518547

HAL Id: hal-01518547

<https://hal.science/hal-01518547>

Submitted on 4 May 2017

HAL is a multi-disciplinary open access archive for the deposit and dissemination of scientific research documents, whether they are published or not. The documents may come from teaching and research institutions in France or abroad, or from public or private research centers.

L'archive ouverte pluridisciplinaire **HAL**, est destinée au dépôt et à la diffusion de documents scientifiques de niveau recherche, publiés ou non, émanant des établissements d'enseignement et de recherche français ou étrangers, des laboratoires publics ou privés.

Wavelet Encoding of BRDFs for Real-Time Rendering

Luc Claustres*

Loïc Barthe†

Mathias Paulin‡

IRIT - University of Toulouse, France

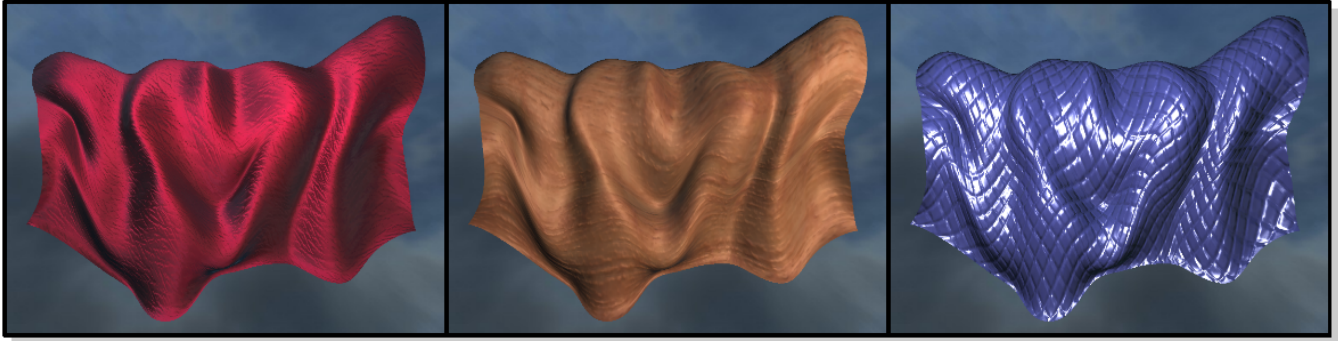


Figure 1: An illuminated fabric with an acquired anisotropic velvet (left), isotropic wood (middle) and shiny plastic (right) BRDF rendered at 40 FPS (512×512) using our wavelet encoding. The initial data sets containing 32^4 RGB samples (12MB) are compressed into 3D textures of 700KB. Our approach can be combined with classical texture, environment and bump mapping in order to produce high quality local illumination.

ABSTRACT

Acquired data often provides the best knowledge of a material's bidirectional reflectance distribution function (BRDF). Its integration into most real-time rendering systems requires both data compression and the implementation of the decompression and filtering stages on contemporary graphics processing units (GPUs). This paper improves the quality of real-time per-pixel lighting on GPUs using a wavelet decomposition of acquired BRDFs. Three-dimensional texture mapping with indexing allows us to efficiently compress the BRDF data by exploiting much of the coherency between hemispherical data. We apply built-in hardware filtering and pixel shader flexibility to perform filtering in the full 4D BRDF domain. Anti-aliasing of specular highlights is performed via a progressive level-of-detail technique built upon the multiresolution of the wavelet encoding. This technique increases rendering performance on distant surfaces while maintaining accurate appearance of close ones.

CR Categories: I.3.7 [Computer Graphics]: Three-Dimensional Graphics and Realism—Color, shading, shadowing, and texture I.3.7 [Computer Graphics]: Picture/Image Generation—Display algorithms

Keywords: brdf, wavelet, real time rendering

1 INTRODUCTION

The past few years have seen impressive improvements in the capabilities of graphics processing units (GPUs). Among many features, the most fascinating achievement is the realisation of GPU

*claustre@irit.fr

†Loic.Barthe@irit.fr

‡Mathias.Paulin@irit.fr

Graphics Interface Conference 2007
28-30 May, Montréal, Canada
Copyright held by authors. Permission granted to CHCCS/SCDHM to publish in print form, and ACM to publish electronically.

programmability for real-time high quality local illumination by directly evaluating physically-based reflection models as each fragment is shaded [25]. These models describe a bidirectional reflectance distribution function (BRDF) defined as the ratio of outgoing radiance to incoming irradiance at a surface point x [32]. The *lighting configuration*, i.e. the *lighting* or *incoming* direction $\omega_i = (\theta_i, \phi_i)$ and the *viewing* or *outgoing* direction $\omega_o = (\theta_o, \phi_o)$, is expressed with spherical coordinates relative to the local coordinate system of the surface (Figure 2). In real-time applications, the direct illumination usually comes from a finite set of N point sources and therefore the general *rendering equation* [13] reduces to:

$$L_o(x, \omega_o) = \sum_{n=1}^N f_r(x, \omega_i^n, \omega_o) \frac{I_n \cos \theta_i^n}{\|x - x_n\|^2}, \quad (1)$$

where L_o is the reflected radiance from a surface point x in the viewing direction, x_n (respectively I_n) is the position (respectively the intensity) of the light source number n , and f_r is the BRDF.

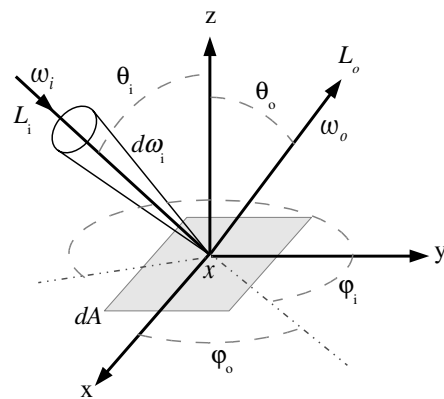


Figure 2: Local surface geometry

Although numerous reflection models have been created [2, 17,



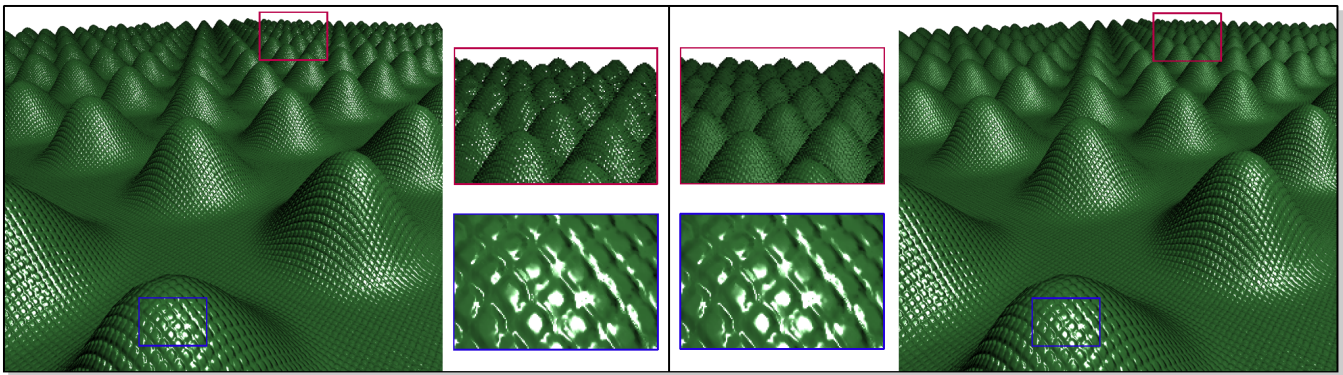


Figure 3: High-frequencies of the BRDF introduce aliasing when the viewpoint is far away from the surface (left image). We perform anti-aliasing, without degrading the appearance of close surfaces, by selecting the appropriate BRDF resolution in the wavelet encoding on a per-pixel basis (right image).

41, 33], a recent experimental analysis [31] has shown that real materials often exhibit a complexity that exceeds the expressive power of current BRDF models. Moreover, the common method of fitting a measured BRDF dataset to analytical models generally requires robust nonlinear optimisation techniques (such as SQP or Levenberg-Marquardt) that are hard to implement and converge slowly. Indeed, low sampling rate and/or noise level make fitting very underconstrained and heavily dependent on the initial guesses. On the other hand, complex models are too computationally expensive for current GPU capabilities. Practical implementation requires to break up the model into separate functions that are sampled and stored in texture maps to avoid direct evaluation [11].

As a consequence, acquired data often provides the best knowledge of the reflectance of a real material. Ideally, on account of the available texture-mapping and computational capabilities of GPUs, we would like a numerical BRDF model that exhibits the following useful features:

- *generality* to handle all-frequency materials (from diffuse to specular),
- *compression* to manage potentially large datasets with controllable error,
- *efficiency* to be evaluated at per-pixel level,
- *filtering* to smoothly reconstruct the BRDF between acquired samples.

2 RELATED WORKS

Recently, bidirectional texture functions (BTFs) [7], modelling realistic acquired materials at pixel scale, have been well studied and produce convincing results [27]. However, the principal component analysis (PCA) [29] used suffers from memory problems during computation and the reconstruction is fast and correct only for relatively simple materials.

Factorisation techniques represent 4D BRDFs using lower-dimensional functions (*factors*) that are multiplied together [9]. Kautz [15] uses a numerical approach based on a singular-value decomposition (SVD) and builds a factorisation of 2D functions. These functions can be stored in texture maps and combined using graphics hardware to perform real-time per-pixel reconstruction. Several improvements have been proposed to optimise the factorisation for GPUs by suppressing negative terms [26], limiting dynamic range, or improving parameterisation [37]. Large

data compression rate can be achieved with factorisation but without flexibility in weighting quality against space. More, these decompositions fail to reproduce fine details (high-frequencies) of a complex material and reconstruction of arbitrary fidelity can require a large number of factors, reducing performances.

Spherical harmonics (SH), which are the Fourier basis functions on the sphere, are often used to represent BRDFs [42]. Indeed, SH are very interesting for shading because their use reduces the lighting integral to a dot product. Nevertheless, SH have global support on the sphere and thus need numerous coefficients to encode general BRDFs. As a consequence, they are restricted to off-line rendering or low-order reconstruction, which can only approximate low-frequency lighting and shadowing effects [30]. On the contrary, Lalonde et al. [18] propose a BRDF representation based on the projection of the data onto a base of 4D *wavelet functions*. Then, a zero-tree encoding is used to efficiently store and evaluate the BRDF. More recently, Claustres et al. introduce the generic wavelet transform [5]. Spectral BRDF datasets are independently projected onto each directional and wavelength dependence using dedicated wavelet transforms. This leads to a better compression ratio according to the reconstruction error.

Precomputed radiance transfer (PRT) [36] aims at enabling real-time illumination with arbitrary BRDFs represented by SH [16], wavelets [22] or factorisation [19]. Interactive rendering including environment lighting, shadowing and interreflections is achieved by pre-computing a sparse light transport matrix per vertex that reduces lighting computations at rendering time. However, because lighting is evaluated per vertex only and interpolated across triangles by graphics hardware, PRT is not well-suited to deal with the high-frequency local illumination induced by realistic materials. It also requires highly tessellated 3D models, prohibitive memory and costly pre-computations.

Discussion: Among these techniques, wavelets exhibit most of the required features. Indeed, an interesting property is the *compact* support of most wavelets, leading to a fast local reconstruction (logarithmic time according to the number of samples). The discrete wavelet transform produces the same number of coefficients as samples in the original dataset, but many of them are close to zero. Flexible lossy compression is obtained by zeroing those that are below a certain threshold. At last, wavelets can handle all-frequency lighting and shadowing effects [30]. For these reasons we propose a wavelet decomposition of the BRDF dataset and implement the reconstruction and filtering stages on the fragment processor, hence providing BRDF-based local illumination with both high-quality and real-time rendering (Figure 1). We also profit from the *multiresolution* (reconstruction at different *levels* of accuracy)



of the wavelet decomposition to improve filtering by performing anti-aliasing of specular highlights (Figure 3).

3 OVERVIEW OF OUR CONTRIBUTION

Our main contribution is a complete numerical BRDF model designed for GPUs, i.e. a *compressed* representation providing reconstruction with *magnification* as well as *minification* filtering in the full 4D BRDF domain in real-time. At the rendering time, the number of texture accesses for each fragment depends on the resolution chosen on-the-fly for the BRDF reconstruction. If the surface is far away from the viewpoint, fewer levels are required to estimate the BRDF and the performance is enhanced. These results are achieved with built-in hardware filtering and by using the linearity and the multiresolution of the wavelet encoding. Moreover, a simple indirection map efficiently compresses BRDF data by removing much of the BRDF correlation between hemispheres corresponding to a set of close directions.

Figure 4 details our BRDF acquisition, encoding and rendering pipeline. First, the BRDF is measured using a gonioreflectometer. Before the wavelet encoding, a pre-process resamples the acquired data to match a regular sampling grid of the BRDF's domain. We complete the sparse dataset using 4D nearest-neighbour queries on directions as done by Schregle [34]. Then, a moving least square (MLS) approximation is applied to smooth the resulting data, reducing measurement noise and discontinuities possibly introduced in the previous pre-processing pass. Next, the wavelet transform is applied in place on the BRDF data, then compression is performed (4). The remaining wavelet coefficients are quantised (5.1) and packed (5.2) into a 3D texture uploaded to the GPU before rendering time. For each pixel in the rendered image, the original BRDF is reconstructed (5.3) from the compressed data with the proper accuracy depending on the distance to the viewpoint (5.4.1). At last, the BRDF samples are filtered in order to produce a smooth lighting solution (5.4.2). This complete pipeline allows modelling and real-time rendering of acquired materials in common graphics applications (6).

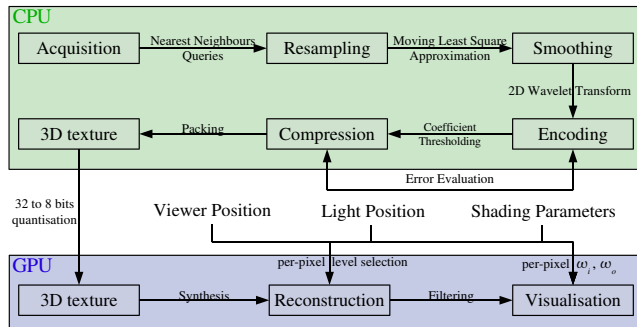


Figure 4: Our BRDF acquisition, encoding and rendering pipeline.

4 WAVELET ENCODING

Wavelets have long been used for data compression, in particular of 2D images, and are the core of the recent JPEG2000 standard [39]. GPU implementations to speed up the transform, e.g. the JasPer codec [40], do exist but decompression occurs on the whole image and not on a per-pixel basis [12]. Although Candussi presents a novel representation of the wavelet coefficient tree amenable to current graphics hardware for 2D data sets [3], compression is limited because the sparse tree is represented as a costly index texture referencing a wavelet coefficient texture. This technique only offers

point sampling, which results in color banding and is not visually acceptable for high-fidelity rendering.

More recently, Garcia et al. reconstruct a wavelet octree at fragment level to perform 3D volume rendering [10]. The 3D data were packed into a huge 2D tileboard where the 3D wavelet reconstruction took place. Similarly, we propose to reconstruct the 4D BRDF data at per-pixel level according to the lighting configuration of a fragment on the viewed surface to produce accurate local illumination. This BRDF data encoding using wavelets theoretically requires a 4D transform. However, previous high-dimension [18] or multiple [5] transforms are not suitable for current graphics processors. On account of the limited capabilities of GPUs, a single wavelet transform could reasonably be implemented, i.e. a transform on incoming *or* outgoing directions \mathbb{S}^2 . Actually, due to the Helmholtz reciprocity principle of BRDFs these transforms are interchangeable.

4.1 Parameterisation

We use an *implicit* approach, which proposes a parameterisation of the sphere, i.e. a mapping between \mathbb{S}^2 and \mathbb{R}^2 , where the transform is more easily expressed. An *explicit* approach, which defines a wavelet transform over the spherical space described as a geometrical mesh [35], has also been explored. An additional *indexing map* must be used at run-time to make the correspondence between directions and triangles by encoding the mesh into textures. This technique suffers from aliasing, requires high-resolution textures to ensure high-quality reconstruction, and makes filtering schemes much more complex.

Lewis [21] recommends the use of Nusselt embedding to compromise on the matter of redundancy at the poles when parameterising the directional component of a BRDF. Christensen [4] prefers to use a combination of a gnomonic projection and stretch to map directions to the unit square. In a real-time context, the cartesian to spherical coordinates transform remains the most obvious and cheap mapping to use though. To limit visual artifacts in our implementation, the poles are aligned with the tangent instead of the normal direction in the local frame of the surface. Indeed, artifacts are less obvious at grazing angles than at front views. This leads to the following mapping: $(x = \sin(\phi) \cos(\theta), y = \cos(\phi), z = \sin(\theta) \sin(\phi))$, with $\theta \in [0, \pi]$ and $\phi \in [0, \pi]$. Another advantage is that both angles are valued in a similar range. Thus, uniform sampling of \mathbb{S}^2 results in a squared grid pattern that simplifies algorithms such as the wavelet transform or data filtering.

4.2 Transform

The transform encodes a set of BRDF samples (hereafter referred to as f_r values) into two parts: the scaling coefficients encoding the smooth *approximation* (low-frequency l values) and the wavelet coefficients encoding the *details* (high-frequency h values), i.e. the missing information to retrieve the original samples from the approximation. The process is recursively repeated on the l values providing a *hierarchical dyadic* decomposition of the samples, i.e. 2^N values lead to N levels or resolutions. We selected the Haar wavelet basis because of its narrow support, which ensures less computational requirements and matches our real-time constraint. Haar's *analysis* and *synthesis* formula for a level number n are given in the following equations:

$$\begin{cases} l_i^{n-1} = \frac{1}{\sqrt{2}}(f_{r_{2i}}^n + f_{r_{2i+1}}^n) \\ h_i^{n-1} = \frac{1}{\sqrt{2}}(f_{r_{2i}}^n - f_{r_{2i+1}}^n) \end{cases} \quad \begin{cases} f_{r_{2i}}^n = \frac{1}{\sqrt{2}}(l_i^{n-1} + h_i^{n-1}) \\ f_{r_{2i+1}}^n = \frac{1}{\sqrt{2}}(l_i^{n-1} - h_i^{n-1}) \end{cases}$$

When the data have multiple dimensions, the most efficient decomposition consists in applying the transform successively on each dimension at each level (*non-standard* approach). Hence local analy-



sis and synthesis are performed in the longitude, then latitude angle, on the nested hemispherical grids (Figure 5).

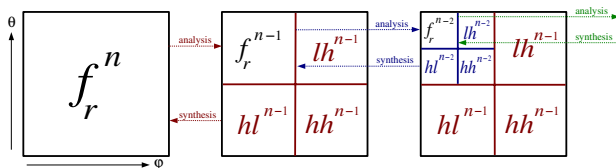


Figure 5: 2D Wavelet transform applied on each hemisphere of the original BRDF data.

4.3 Compression

Claustres et al. have presented in [6] a wavelet compression scheme that generates high compression rates thanks to the computation of an adaptive (local) threshold for each dependence of the BRDF, which is reused in this work. The main idea consists in removing the hemispherical-to-hemispherical BRDF correlation between incoming directions in addition to standard wavelet compression. A set of hemispherical wavelet coefficients is viewed as a vector, which magnitude indicates the relative weight of corresponding hemispherical data in the acquired BRDF. If the vector magnitude lower than a given threshold, all hemispherical coefficients are removed from the wavelet encoding.

Efficient sparse representations of the coefficients usually requires low-level memory access, such as bit masks, and make intensive use of pointers, both techniques are not still available on modern GPUs. More simple indexing techniques, which are easily amenable to graphics processors, are usually not efficient because the memory size of an index (int) or a single coefficient (float) is quite similar. However, using this high-level compression scheme, an index is cheap with regard to a set of hemispherical wavelet coefficients. Thus, indexing becomes efficient as detailed in the next section.

5 WAVELET-BASED BRDF ON GRAPHICS HARDWARE

5.1 Data Quantisation

Precision and dynamic range are potential problems when using a limited precision per color component. Indeed, BRDFs can present arbitrary large dynamic ranges that result in contouring artifacts. To limit this problem, we replace f_r by $\tilde{f}_r = \log\left(\frac{f_r + \epsilon\mu}{\mu}\right)$ as suggested by McCool [26], where μ is the average of all BRDF samples and ϵ a bias factor ensuring strictly positive values. Another advantage is that minimizing RMS error on \tilde{f}_r , results in minimizing relative RMS error on f_r . This is perceptually desirable since the eye is sensitive to ratios of intensity and not absolute intensity. Using this logarithmic encoding, 24-bits per-pixel textures are sufficient as modern GPUs support floating-point precision from end to end of the graphics pipeline. Indeed, it has been acknowledged that wavelet transforms can accommodate low-precision encoding of the coefficients if computations can be done with higher precision [23].

5.2 Data Storage

Since a BRDF is a 4D function, suitable storage would require 4D texture maps. Unfortunately, no commodity hardware currently supports textures with dimensions greater than three. To overcome this limit we organize the 4D BRDF data as a 3D texture where each 2D slice corresponds to a fixed outgoing direction. The normalized incoming latitude and longitude angles computed from the

spherical coordinates of the lighting vector are related to the texture coordinates (s, t) within each slice. The 2D non-standard wavelet transform is applied independently on each slice resulting in a multiresolution texture of wavelet coefficients.

Performing compression then results in suppressing a set of outgoing hemispheres, i.e. vectors of wavelet coefficients, corresponding to a given set of incoming directions. Actually, owing to BRDF reciprocity, this is equivalent to suppress the reciprocal incoming hemispheres, i.e. 2D slices in the 3D texture. The remaining slices are contiguously packed into a new 3D texture with lower depth. An additional *compression map* stores for each slice of the uncompressed texture its corresponding index in the compressed texture. We save this map as a 1D RGB texture encoding 16-bit indices, which is sufficient to handle hemispheres sampled up to $2^8 \times 2^8$ in latitude and longitude angles.

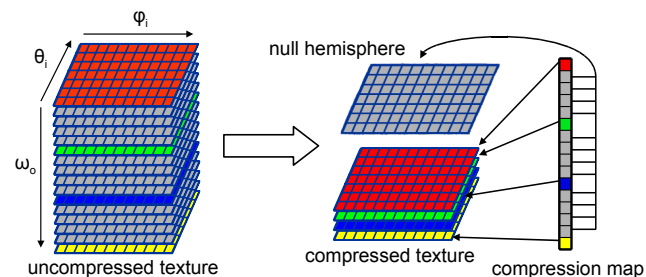


Figure 6: Wavelet coefficient matrix compression. Each gray 2D slice in the original 3D texture is a zeroed outgoing hemisphere removed from the compressed version.

In order to implement zeroing of all wavelet coefficients in the hemisphere, we should effectively remove the corresponding *empty* slice from the 3D texture. Consequently, texture look-up would require branching to test whether the data exists or not. However, branching is only supported on the most recent GPUs and it is only efficient with spatial coherence. Our experiments (restricted to NVIDIA 7x00 GPUs) show that it remains more efficient to avoid branching by referencing a zeroed slice (the same for all the empty hemispheres). This slice is stored as the first 2D slice of the 3D texture and it is referenced by the reserved index 0. The full data organisation is summarized in Figure 6.

Usually, the maximum size of each dimension for 3D textures cannot exceed $2^9(512)$ pixels while 2D textures can often reach $2^{12}(4096)$ pixels. This is problematic for outgoing directions that are stored sequentially in the 3D texture's depth. Indeed, the best sampling allowed is then $2^4 \times 2^4$ in latitude and longitude angles, which is too sparse for most datasets. Fortunately, to reach a better sampling rate, compression by limiting texture depth is worth having.

5.3 Data Reconstruction

For the desired lighting configuration, the synthesis of the BRDF value is done from the lowest resolution, adding more and more details until the highest resolution is reconstructed. At each level, the wavelet coefficients added to refine the current approximation are retrieved from the 3D BRDF texture. Once specified in the uncompressed texture, the texture coordinates are mapped to the compressed version using the compression map (Figure 6). While the (s, t) coordinates of the BRDF texture are directly related to the spherical coordinates of the incoming direction, the third coordinate corresponding to the outgoing direction is computed using a 2D to 1D mapping from the normalised outgoing latitude and longitude angles.



Local BRDF reconstruction requires 2 texture look-ups (longitude then latitude coefficient read) at each level of the decomposition. This number must be doubled as the compressed BRDF texture is indirectly accessed through the compression map. Taking into account the final scaling coefficient read, the total number of look-ups is $4N + 1$ for a N level decomposition. For instance, the local reconstruction of a typical 5-level BRDF requires 21 texture look-ups. Depending on the filtering, several samples have to be reconstructed per-pixel, hence increasing the total number of texture look-ups.

5.4 Data Filtering

5.4.1 Data Minification Filtering

Although the BRDF is invariant with respect to the distance to the camera, sparkling noise may appear due to aliasing of localised high frequencies, i.e. specular highlights (Figure 10). Given the characteristics of an object, Amanatides [1] clamped the shininess of the Phong's BRDF model to values that will not introduce aliasing. Tan [38] uses a Gaussian mixture model, which parameters are pre-computed at different scales and stored into mipmaps to be efficiently evaluated on the GPU at rendering time. Solutions were also proposed for normal maps [14, 8].

BRDF minification filtering theoretically depends on the derivative of the full lighting configuration, where the light/viewer distance and orientation play a role. However, due to singularities in the spherical coordinates system, this is practically difficult to compute. We rather propose to use a simple range-based LOD selection method [28] to obtain a continuous reconstruction level $l \in [0, N - 1[$ on a per-pixel basis when performing rendering. More specifically: $l = \min(\max(\log_2(\alpha d), 0), N - 1)$, where d is the distance from the viewpoint to the rendered fragment and α is a scaling factor. The final BRDF value is linearly interpolated between the value reconstructed at levels $\lfloor l \rfloor$ and $\lfloor l \rfloor + 1$, according to the fractional part of l . This is attractively integrated into our multiresolution encoding, without additional memory requirements. From the number of texture look-ups required for a complete BRDF synthesis, we find that performances are enhanced using the LOD reconstruction when $l < \frac{N-1}{2} + \frac{3}{8}$, otherwise it is more expensive. For instance, rendering becomes faster when $l < 2.375$ for a typical 5-level decomposed BRDF. As a consequence, LOD is interesting in term of performance when most of the pixels are covered by surfaces far away from the viewpoint.

The value of the scaling factor α is typically derived from the bounding volume of the scene and/or a perception-based criterion in order to make the filtering efficient in practical cases. In our experiment, a value of $\alpha = 0.15$ gives good results. Energy conservation, which is a fundamental issue when dealing with realistic reflectance and physically-based illumination, is ensured by the Haar transform. Indeed, for orthonormal wavelet families, e.g. Haar, the total energy in the coefficients is equal to the total energy in the original samples at each scale of the decomposition. For example, the median and mean luminance values computed for both images in Figure 3 are equal. However, as the energy of specular peaks is redistributed on the diffuse component of the BRDF, the scene seems to darken with the LOD used for rendering.

5.4.2 Data Magnification Filtering

A crucial point for the visual realism is the quality of the smooth reconstruction of the BRDF for lighting configurations between acquired samples. Due to the computational complexity of 4D schemes, we share this *magnification* process between built-in hardware bilinear filtering (incoming directions) and software bilinear filtering in the pixel shader (outgoing directions). Indeed, the linearity of the wavelet transform allows us to directly interpolate the

coefficients of the encoded function, without the need of reconstruction. Thus, the final step consists in blending the resulting hardware filtered values in the pixel shader.

6 RESULTS

6.1 BRDF Data

BRDFs are still difficult to acquire, however extensive research is being carried out to provide a better data availability in the future [31, 24, 41]. Up to now, we only have measured the RGB BRDF of different surfaces such as wood, cloth and velvet. We have also used synthetic datasets generated through analytical BRDF models in order to validate our approach. We selected the isotropic model of Lewis [20] and the anisotropic models of Ward [41] and Poulin-Fournier [33].

6.2 Reconstruction Error

Table 1 presents the averaged RMS (ϵ) and relative (ϵ_r) errors for our set of acquired and synthetic BRDFs, with respect to the compression ratio r_c . Initial BRDF resolution of input data is $(32 \times 32)^2$, leading to a BRDF texture of 12MB stored in 32-bits floating point numbers. Evaluation error is always satisfying on the compressed dataset, even for radical thresholding. Results of Ta-

BRDF	Cloth		Wood		Velvet	
Mean value	0.283		0.322		0.323	
r_c	ϵ	ϵ_r (%)	ϵ	ϵ_r (%)	ϵ	ϵ_r (%)
4:1	0.00537	1.64	0.00647	1.70	0.0155	5.22
16:1	0.00930	2.707	0.0133	3.07	0.0321	10.0
32:1	0.0125	3.23	0.0186	3.81	0.0418	12.6
BRDF	Lewis		Ward		Poulin	
Mean value	0.282		0.278		0.394	
r_c	ϵ	ϵ_r (%)	ϵ	ϵ_r (%)	ϵ	ϵ_r (%)
4:1	0.0247	1.74	0.832	2.56	0.0291	12.1
16:1	0.0417	2.90	0.840	4.02	0.0643	20.2
32:1	0.0520	3.73	0.856	6.12	0.0847	26.9

Table 1: Modelling errors for acquired (top) and synthetic (bottom) BRDFs.

ble 1 were achieved by measuring CPU reconstruction error. However, GPU-based BRDF matrices have an additional implicit compression ratio of 4:1 from the 32- to 8-bits data quantisation. The resulting additional error varies between 3% and 8% depending on the datasets. Usually, the final compressed texture used for our real-time applications has a size of less than 1MB, without noticeable visual artifacts.

6.3 Examples

We have implemented the reconstruction algorithm on the NVIDIA GeForce 7800 GTX graphics processor. Vertex and fragment shaders are written in the NVIDIA Cg shading language managed through the OpenGL 2.0 API. The CPU programming has been implemented on an Athlon64 XP3500+ processor running Linux. For a 3-level decomposition, the GPU reconstruction is at least 152 times faster ($\sim 49M$ versus 321K BRDF evaluations per seconds). Even though the use of SIMD extensions of modern CPUs would show a substantial improvement in performance, our gain remains impressive.

Images are computed with a single (but not restricted to) point light source, and the rendering process is separated into two parts. First, a vertex shader program transforms the lighting and viewing



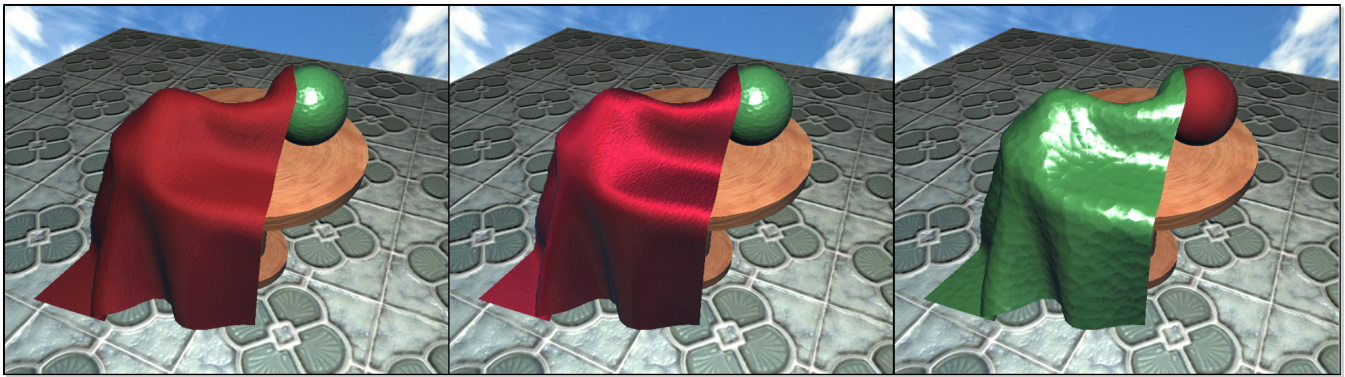


Figure 7: BRDF-based local illumination on a simple scene running at 40 FPS (768 × 768 resolution). From left to right the fabric is mapped with isotropic cloth, anisotropic velvet and high-frequency plastic BRDF. The wood BRDF is applied on the table.

vectors into the local frame of the surface. Then, a fragment shader program computes the final image as follow:

1. determine the reconstruction level based on the distance to the viewpoint;
2. deduce the 3D texture coordinates to access the BRDF texture at required resolution;
3. synthesis of the BRDF value by appropriately weighting coefficients at the different scales;
4. evaluate the lighting equation 1.

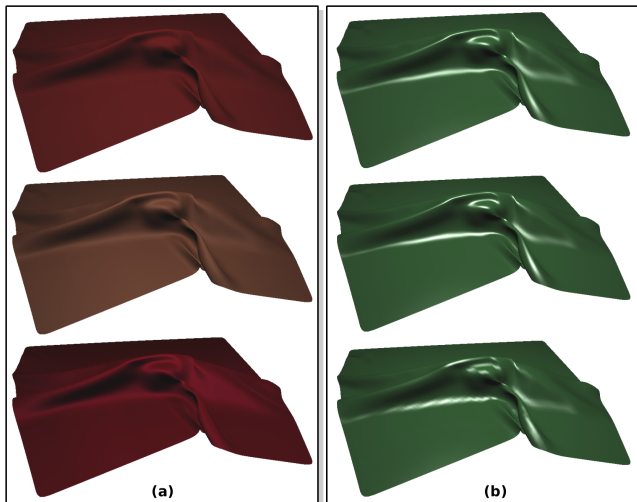


Figure 8: (a) Real-time per-pixel lighting using our wavelet encoding for different acquired BRDFs, from top to bottom: Cloth, Wood and Velvet. (b) Comparison between (top) our approach, (middle) per-pixel lighting using the Lewis analytical BRDF model, and (bottom) per-vertex lighting again using the Lewis model for the same plastic.

Images generated from the acquired BRDFs presented in Table 1 are shown in Figure 8a. Our approximation is also compared with the theoretical BRDF at per-pixel and per-vertex level in Figure 8b. On the fabric model (11K triangles) we have obtained the rates presented in Table 2. Our approach is mainly limited by the number of fragments generated and not by the geometry complexity of the scene. Thus, it can take special advantage of *deferred shading* to

LOD level	0	1	2	3	4
Nearest	390	258	192	152	124
Bilinear	206	90	56	41	31

Table 2: GPU performances (FPS) depending on the data resolution and filtering. Images are generated in a 512×512 floating point pixel buffer. The timing includes the first render pass that reconstructs per-pixel BRDF-based local illumination and the second pass that displays the pixel buffer.

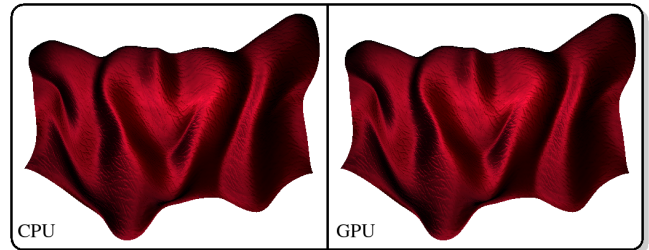


Figure 9: Comparison between our GPU-based approach (right) and a reference lighting solution computed via ray tracing on the CPU (left).

accommodate a large number of vertices or primitives with similar overall performances.

We also compare our BRDF reconstruction and per-pixel lighting on the GPU to a reference lighting solution computed by ray tracing on the CPU (Figure 9). The 3D model (16K triangles) is used with the acquired velvet BRDF, which is our most complex dataset. The mean per-pixel perceptual error ($L^*a^*b^*$ color space) on the resulting images is 1.3 and the corresponding standard deviation 2.29. This demonstrates the rendering accuracy in spite of the data quantisation since an error around 1 in the $L^*a^*b^*$ space is the threshold for non perceptible errors.

Figure 7 illustrates the high-quality local illumination provided by our BRDF representation, mixed with classical bump and environment mapping, for a scene composed of 11K triangles referencing four different BRDFs (velvet, cloth, wood and plastic).

In Figure 10b a terrain scene of 45K triangles is compared with the finest BRDF reconstruction and the LOD reconstruction. For a viewpoint far away from the surface, most specular highlight artifacts are removed by the LOD. The different reconstruction levels used for specular antialiasing are also shown in Figure 10a. The re-



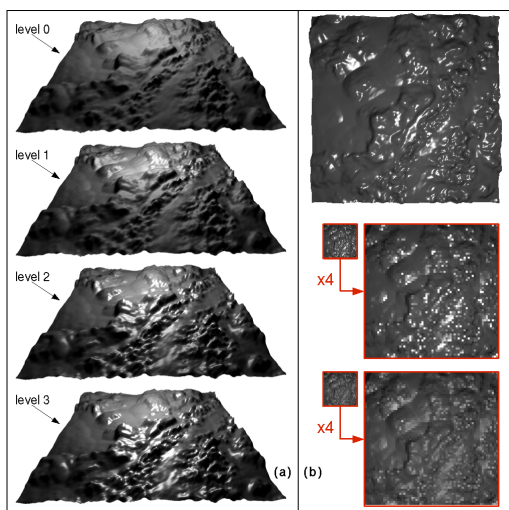


Figure 10: (a) The terrain scene with local illumination reconstructed at different levels. (b) Comparison between BRDF rendering with and without LOD. The landscape model is mapped with the full resolution BRDF on the top. The middle (respectively bottom) part shows the rendering result without (respectively with) LOD. The smaller images are the original displayed on the screen, while the larger are their magnification.

spective acceleration factors compared to the finest approximation level (4) are 1.3, 1.8, 2.7, and 5.7.

7 CONCLUSION AND FUTURE WORK

We have presented an efficient BRDF representation based on wavelets for acquired data. This representation is suitable for real-time reconstruction using graphics hardware and per-pixel local illumination with general (anisotropic) BRDFs. BRDF data are stored into moderate-resolution 3D textures (typically $32 \times 32 \times 256$) and thus a scene may contain many different BRDFs. We provide a novel multiresolution representation that allows the real-time rendering of BRDF at different LODs and the filtering of specular highlights without additional memory cost.

We plan to improve the fine detail reconstruction by using other wavelets than Haars', certainly at the cost of slower reconstruction. Coherence between reconstruction at different levels could also be exploited to avoid redundant computations and texture look-ups when performing LOD.

REFERENCES

- [1] John Amanatides. Algorithms for the detection and elimination of specular aliasing. In *Proceedings of the conference on Graphics interface '92*, pages 86–93, San Francisco, CA, USA, 1992. Morgan Kaufmann Publishers Inc.
- [2] M. Ashikhmin and P. Shirley. An Anisotropic Phong BRDF Model. *Journal of Graphics Tools*, 5(2):25–32, 2000.
- [3] N. Candussi, S. DiVerdi, and T. Hollerer. Real-time rendering with wavelet-compressed multi-dimensional textures on the gpu. Technical Report 2005-05, Department of Computer Science, University of California, Carolina, January 2005.
- [4] Per H. Christensen, Eric J. Stollnitz, David H. Salesin, and Tony D. DeRose. Global Illumination of Glossy Environments Using Wavelets and Importance. *ACM Transactions on Graphics*, 15(1):37–71, January 1996.

- [5] L. Claustres, M. Paulin, and Y. Boucher. BRDF Measurement Modelling using Wavelets for Efficient Path Tracing. *Computer Graphics Forum*, 22(4):701–716, 2003.
- [6] L. Claustres, M. Paulin, and Y. Boucher. A Wavelet-Based Framework for Acquired Radiometric Quantity Representation and Accurate Physical Rendering. *The Visual Computer*, 22(4):221–237, 2006.
- [7] K. J. Dana, B. Van Ginneken, S. K. Nayar, and J. J. Koenderink. Reflectance and Texture of Real World Surfaces. *ACM Transactions on Graphics*, 18(1):1–34, 1999.
- [8] A. Fournier. Normal distribution functions and multiple surfaces. In *Graphics Interface 92 Workshop on Local Illumination*, pages 45–52, 1992.
- [9] Alain Fournier. Separating Reflection Functions for Linear Radiosity. In P. M. Hanrahan and W. Purgathofer, editors, *Rendering Techniques '95 (Proceedings of the Sixth Eurographics Workshop on Rendering)*, pages 296–305. Springer-Verlag, 1995.
- [10] Antonio Garcia and Han-Wei Shen. GPU-based 3D wavelet reconstruction with tileboarding. In *Proceedings of Pacific Graphics 2005*, pages 755–763, 2005.
- [11] Wolfgang Heidrich and Hans-Peter Seidel. Realistic, hardware-accelerated shading and lighting. In *Computer Graphics Proceedings, Annual Conference Series (Proc. SIGGRAPH '99)*, pages 165–171, August 1999.
- [12] M. Hopf and T. Ertl. Hardware Accelerated Wavelet Transformations. In *Proc. EG/IEEE TCVG Symposium on Visualization VisSym 2000*, pages 93–103, 2000.
- [13] James T. Kajiya. The Rendering Equation. In *Computer Graphics (ACM SIGGRAPH '86 Proceedings)*, volume 20, pages 143–150, August 1986.
- [14] J. Kautz, W. Heidrich, and H.P. Seidel. Real-time bump map synthesis. In *HWWS '01: Proceedings of the ACM SIGGRAPH/EUROGRAPHICS workshop on Graphics hardware*, pages 109–114, New York, NY, USA, 2001. ACM Press.
- [15] J. Kautz and M. D. McCool. Interactive rendering with arbitrary BRDFs using separable approximations. In *Rendering Techniques '99*, pages 247–260. Springer Wien, 1999.
- [16] J. Kautz, P.P. Sloan, and J. Snyder. Fast, arbitrary brdf shading for low-frequency lighting using spherical harmonics. In *Proceedings of the 12th Eurographics Workshop on Rendering*, pages 301–308, 2002.
- [17] Eric P. Lafortune, Sing-Choong Foo, Kenneth E. Torrance, and Donald P. Greenberg. Non-linear approximation of reflectance functions. In *Computer Graphics (ACM SIGGRAPH '97 Proceedings)*, volume 31, pages 117–126, 1997.
- [18] P. Lalonde and A. Fournier. A wavelet representation of reflectance functions. *IEEE Transactions on Visualization and Computer Graphics*, 3(4):329–336, August 1997.
- [19] Lutz Latta and Andreas Kolb. Homomorphic factorization of BRDF-based lighting computation. *ACM Transactions of Graphics (Proceedings of SIGGRAPH 2002 Annual Conference)*, 21(3):509–516, 2002.
- [20] Robert R. Lewis. Making Shaders More Physically Plausible. In *Fourth Eurographics Workshop on Rendering*, pages 47–62, Paris, France, June 1993.
- [21] Robert R. Lewis. *Light-Driven Global Illumination with a Wavelet Representation of Light Transport*. PhD thesis, Department of Computer Science, University of British Columbia, Vancouver, British Columbia, 1998. Available from <http://www.cs.ubc.ca/labs/imager/th/lewis.phd.1998.html>.
- [22] Xinguo Liu, Peter-Pike Sloan, Heung-Yeung Shum, and John Snyder. All-frequency precomputed radiance transfer for glossy objects. In A. Keller and H. W. Jensen, editors, *Proceedings of Eurographics Symposium on Rendering 2004*, pages 337–344, June 2004.
- [23] S. Mallat. *A Wavelet Tour of Signal Processing*. Academic Press, San Diego, 1999.
- [24] Matusik, W. H. Pfister, M. Brand, and L. McMillan. Efficient Isotropic BRDF Measurement. In *Proceedings of Eurographics Symposium on Rendering 2003*, pages 241–247, 2003.
- [25] D. McAllister, A. Lastra, and W. Heidrich. Efficient rendering of spatial bi-directional reflectance distribution functions. In *Proceedings of the Eurographics/SIGGRAPH Workshop on Graphics Hardware 2002*, 2002.



- [26] Michael D. McCool, Jason Ang, and Anis Ahmad. Homomorphic factorization of BRDFs for high-performance rendering. In *Computer Graphics Proceedings, Annual Conference Series (SIGGRAPH 2001)*, August 2001.
- [27] J. Meseth, G. Muller, and R. Klein. Reflectance field based real-time, high-quality rendering of bidirectional texture functions. *Computers and Graphics*, 28(1):103–112, 2004.
- [28] Tomas Moller and Eric Haines. *Real-Time Rendering*. A. K. Peters Limited, 1999.
- [29] G. Muller, J. Meseth, and R. Klein. Compression and Real-Time Rendering of Measured BTFs Using Local PCA. In *Proceedings of Vision, Modeling and Visualisation 2003*, pages 271–280, 2003.
- [30] R. Ng, R. Ramamoorthi, and P. Hanrahan. All-frequency shadows using non-linear wavelet lighting approximation. *ACM Trans. Graph.*, 22(3):376–381, 2003.
- [31] A. Ngan, F. Durand, and W. Matusik. Experimental Analysis of BRDF Models. In *Proceedings of Eurographics Symposium on Rendering 2005*, pages 117–226, 2005.
- [32] F. E. Nicodemus, J. C. Richmond, J. J. Hsia, I. W. Ginsberg, and T. Limperis. Geometric Considerations and Nomenclature for Reflectance. Monograph 161, National Bureau of Standards (US), October 1977.
- [33] P. Poulin and A. Fournier. A Model for Anisotropic Reflection. *Computer Graphics*, 24(4):273–282, 1990.
- [34] R. Schregle and J. Wienold. Physical Validation of Global Illumination Methods: Measurement and Error Analysis. *Computer Graphics Forum*, 23(4):761–781, 2004.
- [35] Peter Schroder and Wim Sweldens. Spherical Wavelets: Efficiently Representing Functions on the Sphere. In *Computer Graphics Proceedings, Annual Conference Series, 1995 (ACM SIGGRAPH '95 Proceedings)*, pages 161–172, 1995.
- [36] Peter-Pike Sloan, Jan Kautz, and John Snyder. Precomputed radiance transfer for real-time rendering in dynamic, low-frequency lighting environments. *ACM Transactions on Graphics (Proceedings of SIGGRAPH 2002 Annual Conference)*, 21(3):527–536, 2002.
- [37] F. Suykens, K. Berge, A. Lagae, and P. Dutre. Interactive Rendering with Bidirectional Texture Functions. *Computer Graphics Forum*, 22(3):463–472, 2003.
- [38] P. Tan, S. Lin, L. Quan, B. Guo, and H.-Y. Shum. Multiresolution Reflectance Filtering. In *Proceedings of Eurographics Symposium on Rendering 2005*, pages 111–116, 2005.
- [39] D.S. Taubman and M.W. Marcellin. *JPEG2000 : Image Compression Fundamentals, Standards and Practice*. Kluwer Academic Publishers, 2001.
- [40] J. Wang, T. T. Wong, P. A. Heng, and C. S. Leung. Discrete Wavelet Transform on GPU. In *Proceedings of ACM Workshop on General Purpose Computing on Graphics Processors*, pages C–41, 2004.
- [41] Gregory J. Ward. Measuring and Modeling Anisotropic Reflection. In *Computer Graphics (ACM SIGGRAPH '92 Proceedings)*, volume 26, pages 265–272, July 1992.
- [42] Stephen H. Westin, James R. Arvo, and Kenneth E. Torrance. Predicting Reflectance Functions From Complex Surfaces. In *Computer Graphics (ACM SIGGRAPH '92 Proceedings)*, volume 26, pages 255–264, July 1992.

